Magnetization model for geothermal exploration

Title:
Magnetization model for geothermal exploration

Document no.:	Contract no.:	Project: **DEEPEN**

Classification: **Open**	Distribution:
Expiry date:	Status: **Draft**

Distribution date: **10.02.2022**	Rev. no.:	Copy no.:

Author(s)/Source(s): **Ketil Hokstad and Claudia Kruber**	
Subjects: Magnetization, oxidation, solid exsolution, Ising model, Curie temperature, geothermal exploration, deep-sea minerals	
Remarks:	
Valid from:	Updated:
Responsible publisher:	Authority to approve deviations:

Prepared by (Organisation unit / Name): Ketil Hokstad	Date/Signature: X
Responsible (Organisation unit/ Name):	Date/Signature: X
Recommended (Organisation unit/ Name):	Date/Signature: X
Approved by (Organisation unit/ Name):	Date/Signature: X

Summary

Rock magnetism and magnetic potential field data are influenced by many factors, including mineral composition, hydrothermal alteration, faults, and past and present temperatures. Laboratory measurements on rock samples from the Reykjanes and Hellisheidi geothermal areas on Iceland show that midoceanic-ridge basalts possess large remanent magnetization with two or three different Curie temperatures.

The primary magnetic carrier in basalt is titanomagnetite. The magnetic properties are subsequently altered by solid exsolution and oxidation due to interaction between the rock and hydrothermal fluids. A quantitative model for magnetization in basalt is presented. The model combines well-known models and concepts:

1. The Ising model, which captures both the remanent and induced part of magnetization,
2. Mixed 1st and 2nd order Arrhenius kinetics
3. A thermodynamic model, for spinodal exsolution

The purpose of the model is to capture 1st order effects, such that the model is applicable to inversion of magnetic potential-field data, multigeophysical inversion, machine learning, and geothermal exploration. The model is demonstrated on a temperature vs depth curve from the IDDP-2 well at Reykjanes, and a 3D temperature cube from the Hellisheid/Nesjavellir geothermal area.

The magnetic model is also relevant for deep-sea mineral exploration.

Table of contents

1 Introduction

The magnetic properties of mid-oceanic ridge basalts have been studied extensively since the classical work of Vine and Matthews (1963). They proposed that the alternating pattern of seabed lineaments with positive and negative magnetization was associated with sea-floor spreading and reversals of the earth magnetic field. This complicates the analysis of rock magnetism for rocks that have experienced several flips of the magnetic field and tectonic movement away from the position of crystallization of the rock. Young basalts from places like Iceland are of special interest for magnetic studies, since these complications are less severe. Also, such investigations are of interest from a geothermal and deep-sea mineral exploration point of view.

The magnetization of minerals and rocks can be seen as a battle between quantum-mechanical order at low temperatures and thermal disorder at high temperatures. The transition between these two domains take place around the Curie/Neel temperature. Below the Curie temperature the rock is ferromagnetic (Curie) or ferrimagnetic (Neel). Above the Curie temperature, only a weak paramagnetism or diamagnetism remains. This transition is captured by the Ising (1925) model from quantum statistics, which represents both remanent magnetization due to spin-spin interactions, and induced magnetization due to spin interaction with an external field.

The main carriers of magnetism in mid-oceanic ridge basalts (MORB) are iron-titanium oxides (Pariso and Johnsen, 1991). In fresh oceanic crust, the primary magnetic mineral is titanomagnetite (TM) with approximately 60% ulvöspinel, often referred to as TM60. When magma cools, titanomagnetite crystalizes around 1200-1300 degrees, relatively early in the crystallization sequence that forms igneous rocks. At high temperatures, titanomagnetite, belonging to the spinel group, forms a solid solution of ulvöspinel and magnetite (Smith, 1980). When the rock cools below $\sim 600\ ^{o}C$, the titanomagnetite becomes unstable, associated with a miscibility gap in the phase diagram. Consequently, the initially homogeneous titanomagnetite decomposes into phases enriched in ulvöspinel and magnetite (MT), respectively, and with two different Curie temperatures (Yund and McAllister, 1969; Wise et al., 2011; Lattard et al., 2006).

The titanomagnetite is subject to chemical alteration. This is a complicated process, depending on temperature, cooling rate and oxygen fugacity. However, two main stages have been identified (Pariso and Johnson, 1991, Lattard et al., 2005). First, high-temperature oxidation takes place before and while the lava solidifies, at temperatures above $600 - 700\ ^{o}C$, and hence, above the Curie temperature of magnetite. Ulvöspinel is the least stable compound of the titanomagnetite. Therefore, the main effect of the high-temperature oxidation is to produce titanomagnetite enriched in magnetite, and with grains subdivided by ilmenite lamellae (Johnson and Hall, 1978; Oliva-Urcia et al., 2011).

Second, low-temperature oxidation takes place after the lava solidifies, at temperatures below $\sim 350\ ^{o}C$ (Zhou et al., 2001; Oliva-Urcia, et al., 2011). This involves the interaction of rocks and hydrothermal fluids, and is enhanced in aqueous environments (Ade-Hall et al., 1971). The main alteration product is titanomaghemite (TMGH) with a Curie temperature in the range $200 - 450\ ^{o}C$, depending on the degree of oxidation (Moskowitz and Banerjee, 1981, Xu et al., 1997). In titanomaghemite, the initial spinel structure of the titanomagnetite is preserved, but with a cation-deficient lattice (Gapeev and Gribov, 1990).

Dietze et al (2010) analyzed rock samples from the Reykjanes geothermal area and observed three and sometimes four different Curie temperatures in each sample. Similar observations were made by Oliva-Urcia et al (2011) at Krafla, and in a study by NTNU performed on samples collected by Equinor in the Hellisheidi geothermal area (ter Maat and Church, 2020, unpublished). All three studies, however, were done on surface samples or rocks samples from shallow wells and does not necessarily describe magnetic properties at greater depths.

The development of multiple Curie temperatures in basaltic rocks can be explained by a combination of oxidation and/or exsolution of titanomagnetites. The Curie temperature acts like fingerprint for magnetic minerals (Butler, 1992). In the present work, we develop a quantitative model for magnetization incorporating such effects. The purpose of developing this model is to include magnetic data and magnetization in multigeophysical inversion to estimate properties of interest; primarily subsurface temperature and porosity (Hokstad et al., 2017, Hokstad and Tänavsuu-Milkeviciene, 2017; Hokstad et al. 2020). To make the magnetization model applicable to geothermal exploration, we focus on first order generic effects, while ignoring second order effects that are difficult to control without drilling and coring.

2 Magnetization

Magnetic anomaly data are due to dipole sources in the subsurface. The anomalous magnetic field vector $\boldsymbol{B_A}$ can be expressed as a double differentiation of an inverse-distance potential (Blakely, 1996)

$$\boldsymbol{B_A}(\boldsymbol{x}) = -\frac{\boldsymbol{\mu_0}}{\boldsymbol{4\pi}}\boldsymbol{\nabla\nabla}\cdot\iiint\frac{\boldsymbol{M}(\boldsymbol{x'})}{|\boldsymbol{x'}-\boldsymbol{x}|}\boldsymbol{dV'}, \tag{1}$$

where $\boldsymbol{M}$ is the magnetization vector, $\boldsymbol{x'} = (x', y', z')$ denotes the positions of magnetic sources, $\boldsymbol{x} = (x, y, z)$ is the position where the magnetic field is observed, μ_0 is the vacuum permeability, and $dV' = dx'dy'dz'$ is the volume differential.

The magnetization in rocks consists of two parts, remanent magnetization $\boldsymbol{M_R}$ and induced magnetization $\boldsymbol{M_I}$, such that

$$\boldsymbol{M} = \boldsymbol{M_R} + \boldsymbol{M_I} = \boldsymbol{M_R} + \boldsymbol{\chi H}, \tag{2}$$

where χ is the magnetic susceptibility, and $\boldsymbol{H}$ is the inducing field. Physically, the magnetization represents magnetic dipole moment per unit volume, with SI-units A/m. The Königsberger ratio $Q_k = M_R/\chi H$ is a measure of the relative importance of remanent and induced magnetization.

The main carrier of magnetization in basaltic oceanic crust is iron-titanium oxides. The initial magnetic mineral is titanomagnetite, with chemical formula $Fe_{3-u}Ti_uO_4$, belonging to the spinel group. The titanomagnetites in fresh oceanic crust exhibits a rather uniform composition, with 60% ulvöspinel ($u = 0.6$) and 40% magnetite (Butler, 1992; Pariso and Johnson, 1991). The volume fraction of iron-titanium oxides in basaltic rocks is typically $\sim 5\%$ (Butler, 1992).

When lava cools and solidifies, significant changes of magnetic properties may take place (*Figure 1*). Processes with major influence on magnetic properties are

1. High temperature (deuteric) oxidation (Butler, 1992; Steinthorsson and Sveinbjørnsdottir, 1981)
2. Low temperature (hydrothermal) oxidation (Ade-Hall et al., 1971; Prevot et al., 1981, Gapeev and Gribov, 1990; Zhou et al., 2001; Oliva-Urcia et al., 2011)
3. Solid exsolution (Yund and McAllister, 1969; Wise et al., 2011; Hokstad et al., 2020)

These processes will be discussed below. Low-temperature oxidation and solid exsolution are then put together in a quantitative forward model for magnetization.

The main purpose of developing a forward model for magnetization, is to apply the model in **multigeophysical inversion** and **machine learning** for geothermal exploration.

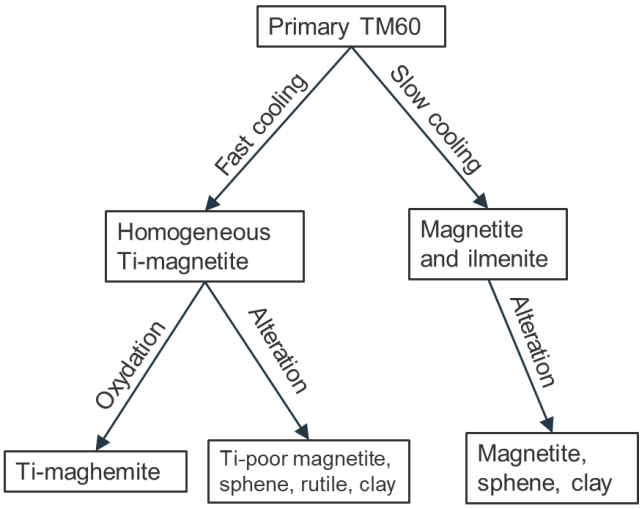

***Figure 1**: Possible cooling and alteration histories of primary titanomagnetite grains. Adapted and simplified from Pariso and Johnsen (1991). The main focus of the present work is the left branch; with fast cooling and oxidation.*

3 Curie temperature

The Curie temperature is the critical temperature for ferromagnetism. The corresponding property for antiferromagnetic and ferrimagnetic materials is called Neel temperature. Near the Curie/Neel temperature, materials lose their permanent magnetization, and become paramagnetic. In the following, the name Curie temperature will be used for simplicity. The Curie temperature acts like a fingerprint of many minerals. For instance, the Curie temperature for magnetite, which is a ferrimagnetic mineral, is $T_c \simeq 570\ ^oC$, and for ulvöspinel it is $T_c \simeq -150\ ^oC$. For titanomagnetite, the Curie temperature varies between the two limiting values, depending on the ulvöspinel fraction (*Figure* ***2***).

Dietze et al. (2010) presented a study from the Reykjanes Peninsula, and concluded that titanomagnetite with small grain sizes is the main carrier of magnetization. They analyzed magnetic properties of rock samples, and related small-scale properties to magnetic potential field measurements. Laboratory measurements of susceptibility vs temperature show that two or sometimes three different Curie temperatures, between 30 ºC and 570 ºC can be found in each rock sample. Oliva Urcia et al. (2011) made similar observations in a study on rock samples from Krafla, Iceland. In 2019, Equinor performed fieldwork in the Hellisheid/Nesjavellir geothermal area, discussed in more detail in Section 10 below. Analysis of basalt samples from Hellisheidi gave results resembling the observations of Dietze et al. (2010) and Oliva Urcia et al. (2011). Multiple Curie temperatures can be explained by solid exsolution of titanomagnetite and/or oxidation of titanomagnetite to form titanomaghemite.

Based on laboratory studies on synthetic titanomagnetites, Lattard et al (2006) obtained the relation (*Figure* ***2***a)

$$\boldsymbol{T_c^{TM} = -150u^2 - 580u + 851.} \tag{3}$$

where u is the ulvöspinel fraction, and T_c^{TM} is in Kelvin. For titanomaghemite, the Curie temperature depends on the degree of oxidation. Based on the data published by Moskowitz and Banerjee (1981), an empirical equation for the Curie temperature of titanomaghemite T_c^{TMGH} (Kelvin) can be expressed as (*Figure* ***2***b)

$$\boldsymbol{T_c^{TMGH} = -110z^2 + 480z + 475,} \tag{4}$$

where z is the degree of oxidation.

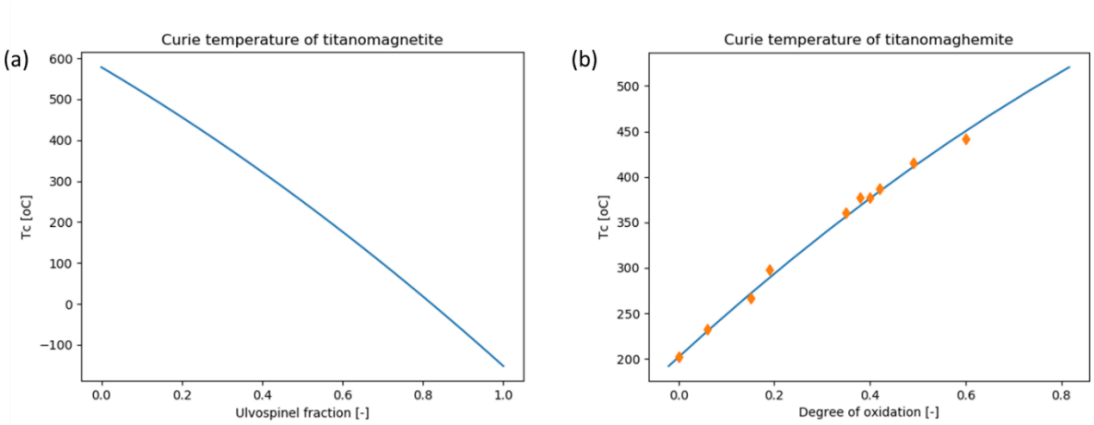

Figure 2. (a) Curie temperature of titanomagnetite vs ulvöspinel fraction presented by Lattard et al., 2006. (b) Curie temperature of titanomaghemite vs degree of oxidation, based on data from Moskowitz and Banerjee (1981) shown as orange diamonds. The Curie temperatures are displayed in Celsius degrees.

4 Ising model

On the microscopic level, magnetization can be explained as spin interactions, both internal spin-spin interactions, and interactions between spin and an external magnetic field. To describe the thermal effects on magnetization, we want a simple model that links quantum effects to the macroscopic magnetization. Here, as a phenomenological model, we use the one-dimensional (1D) Ising (1925) model from quantum statistics. In the Ising model, the Hamiltonian $\boldsymbol{\varepsilon}$ (energy) for a system of particles with interacting spins σ_j and under the influence of an external magnetic field H is given by

$$\boldsymbol{\varepsilon} = -\boldsymbol{J}\sum_{<ij>}\boldsymbol{\sigma_i}\,\boldsymbol{\sigma_j} - \boldsymbol{\mu_B H}\sum_{j}\boldsymbol{\sigma_j}, \tag{5}$$

where μ_B is the magnetic moment of each particle, J is the inter-particle interaction strength, and the notation $< ij >$ means that the sum runs over all nearest-neighbor combinations. In Hamiltonain, the first term represents remanent magnetization, and the second term induced magnetization.

After some algebra, using methods of statistical mechanics and assuming the Boltzmann distribution, the macroscopic magnetization of a large ensemble of particles can be written as

$$\frac{\boldsymbol{M}}{\boldsymbol{M_0}} = \tanh\left[\frac{\boldsymbol{T_C M}}{\boldsymbol{T M_0}} + \frac{\boldsymbol{CH}}{\boldsymbol{T M_0}}\right], \tag{6}$$

where M is the magnitude of the total magnetization vector (remanent plus induced), M_0 is the magnetization at absolute zero, T is the temperature (Kelvin), T_C is the Curie temperature (Kelvin), and C is the Curie constant. Equation (**6** is transcendental and can be solved graphically or numerically. The susceptibility is given by

$$\boldsymbol{\chi} = \frac{\boldsymbol{M(T,H)} - \boldsymbol{M(T,0)}}{\boldsymbol{H}}, \tag{7}$$

where $M(T,0) = M_R$ is the remanent magnetization in the absence of an external field. For high temperatures, Equation(**7** can be linearized, which leads to the well-known Curie-Weiss law

$$\boldsymbol{\chi} \simeq \frac{\boldsymbol{C}}{\boldsymbol{T - T_C}}. \tag{8}$$

The Ising model can be used to represent the magnetic properties of a homogeneous single-domain magnetic phase. We approximate a heterogeneous mix of magnetic phases, by a linear combination of single-phase models (Equation (**6**),

$$\boldsymbol{M(T)} = \sum_j \boldsymbol{w_j M_j(T)}, \tag{9}$$

where w_j is the weight of phase *j*. The linear superposition is supported by the linearity in magnetization of the magnetostatic Equation (**1**.

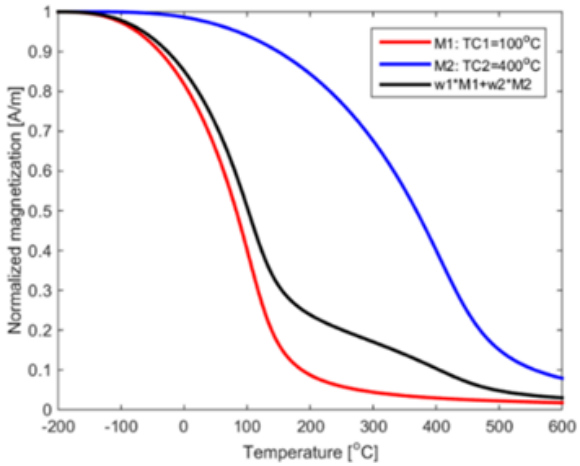

Figure 3. Two Ising models with different Curie temperatures $\boldsymbol{T_{C1} = 100}$ *°C (red) and* $\boldsymbol{T_{C2} = 400}$ *°C (blue), and the superposition of the two models (black).*

5 High-temperature oxidation

Titanomagnetite crystalizes at a temperature $T \sim 1300^oC$, and is among the first minerals to crystalize in the cooling and crystallization sequence of igneous rocks. The grain size of magnetic minerals depends on the cooling rate. Slow cooling leads to larger grains (up to 100 μm), and fast cooling gives smaller grains ($\sim 1\ \mu m$). Fine grain titanomagnetites are the best magnetic recorders, and often develop pseudo-single domain magnetic structure (Butler, 1992, Prevot et al, 1981)

High-temperature, deuteric oxidation takes place right before and while basaltic rocks solidify, at temperature above 700^oC, and hence above the Curie temperature of magnetite. Oxygen fugacity needs to be $f_{O_2} \geq 10^{-7}$ MPa. Ilmenite ($\alpha FeTiO_3$) lamellae are expelled, and consequently, the host titanomagnetite is enriched in magnetite. An equilibrium dependending on temperature and oxygen fugacity can be written as (Lattard et al., 2005)

$$\boldsymbol{Fe_2TiO_4 + Fe_2O_3 = FeTiO_3 + Fe_3O_4}, \tag{10}$$

subject to the oxygen buffer

$$4Fe_3O_3 + O_2 = 6Fe_2O_3. \tag{11}$$

The ilmenite lamellae subdivide the initial titanomagnetite into smaller grains. Ilmenite is a paramagnetic mineral that does not contribute significantly to the magnetization. In the case of extreme deuteric oxidation, the oxidation products can be rutile (TiO_2), hematite (αFe_2O_3), and pseudobrookite (Fe_2TiO_5). The oxidation products occupy a smaller volume than the initial titanomagnetite, which leads to shrinkage cracks, and (slightly) increased porosity.

6 Low-temperature oxidation

Low-temperature oxidation of titanomagnetite occurs after solidification of the basaltic rocks, typically at temperatures $T < 350\ ^oC$. The main alteration process taking place is maghemitization due to fluid-rock interaction. Relevant processes for geothermal and deep-sea mineral exploration are (Oliva-Urcia et al., 2011)

1. Formation of titanomaghemite under oxidizing conditions.
2. Formation of pyrite (and chalcopyrite) under acidic conditions.

Titanomaghemite belongs to the spinel group, but is cation deficient since Fe^{2+} ions migrate out of the spinel lattice. The chemical formula of titanomaghemite is $\gamma FeTiO_3$, which collapses to $\alpha FeTiO_3$ (ilmenite), with a hexagonal structure, at temperatures $T > 400\ ^oC$.

The (non-unique) chemical process creating titanomaghemite can be written as

$$Fe_2TiO_4 + 2H^+ \rightarrow FeTiO_3 + Fe^{2+} + H_2O \tag{12}$$

A possible subsequent (non-unique) formation of sulfide minerals is given by

$$\begin{gathered} 2H_2S + Fe^{2+} \rightarrow FeS_2 + 2H^+ \\ ZnCl_2 + H_2S \rightarrow ZnS + 2HCl \\ 2H_2S + Fe^{2+} + CuCl_2 \rightarrow CuFeS_2 + 2HCl + 2H^+ \end{gathered} \tag{13}$$

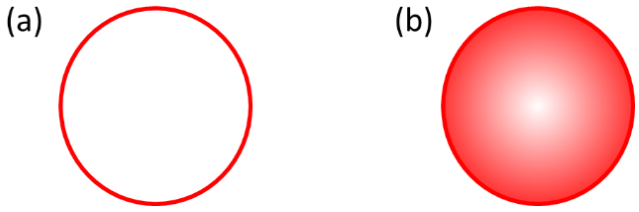

Figure 4. *Conceptual model for maghemitization of titanomagnetite in two stages. a) Fast oxidation of the surface of the grain. b) Slow diffusive oxidation of the interior of the grain.*

The maghemitization of titanomagnetite takes place in two stages (*Figure 4*). First, a thin oxidized layer forms at the rim of the titanomagnetite grain. This process is relatively fast, and with relatively small activation energy E_1. The rate is controlled by the Arrhenius equation,

$$k_1 = Ae^{-\frac{E_1}{RT}}, \tag{14}$$

where T is absolute temperature (in Kelvin), and R is the gas constant. Gapeev and Gribov (1990) found experimentally the activation energies for varying initial ulvöspinel fraction u and degrees of oxidation z (*Figure 5*).

Second, the oxidation progress inward, into the titanomagnetite grains by a slower diffusion process. This process was analyzed theoretically by Fabian and Shcherbakov (2020), who suggested a linear increase in activation energy with increasing degree of oxidation,

$$E_2(z) = E_1 + \mu z, \tag{15}$$

where $\mu \sim 135$ kJ/mol is the gradient of the activation energy, and the rate of the diffusive stage is given by

$$k_2 = Ae^{-\frac{E_2}{RT}}. \tag{16}$$

The reaction frequencies A depend on the grain size, which is unknown in an exploration setting, and hence, this is subject to local empirical calibration.

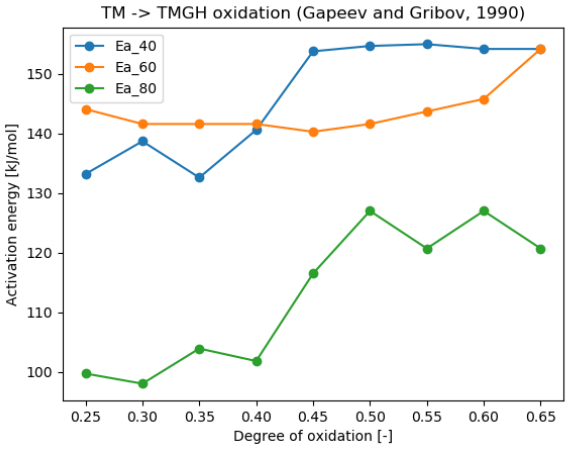

Figure 5. Activation energy for maghemitization of titanomagnetite for initial ulvöspinel fractions $\boldsymbol{u = 0.4, 0.6, 0.8}$ *and varying degrees of oxidation. Data from Gapeev and Gribov (1990).*

We propose a simple kinetic model for oxidation which is a weighted average of fast and slow first order reactions (*Figure 6*), controlled by k_1 and k_2. Hence, in the limits of $x \simeq x_0$ and $x \to 0$, respectively, the kinetic model should reduce to

$$\frac{dx}{dt} = -k_1 x, \qquad (\text{when } t \simeq t_0, x \simeq x_0) \tag{17}$$

$$\frac{dx}{dt} = -k_2 x, \qquad (\text{when } t \to \infty, x \to 0) \tag{18}$$

where x is the volume fraction (concentration), of titanomagnetite (with ulvöspinel fraction u and magnetite fraction $1 - u$). A model that fulfils the above conditions can be written as

$$\frac{dx}{dt} = -a_1 k_1 x - a_2 k_2 x \tag{19}$$

with normalized weights a_1 and a_2 given by

$$a_1 = \frac{x}{x_0}, \tag{20}$$

$$a_2 = \frac{x_0 - x}{x_0}. \tag{21}$$

This effectively leads to a mixed 1st and 2nd order kinetic model which can be rewritten as

$$\frac{dx}{dt} = -\left(\frac{k_1 - k_2}{x_0}\right)x^2 - k_2 x. \tag{22}$$

For constant temperature, and hence constant rates k_1 and k_2, the mixed order kinetic equation can be solved analytically, giving

$$x(t) = \frac{x_0 e^{-k_2 t}}{1 + \frac{k_1 - k_2}{k_2}(1 - e^{-k_2 t})}. \tag{23}$$

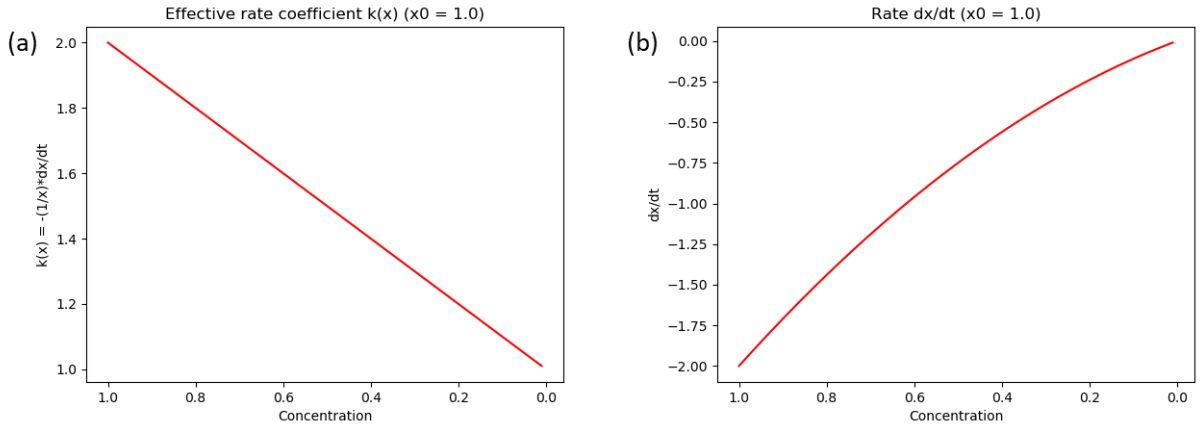

Figure 6. Effective mixed 1st and 2nd order kinetic model. (a) Effective rate coefficient $\boldsymbol{k_{eff}(x) = -(1/x)dx/dt}$ *and (b) rate of change of concentration* $\boldsymbol{dx/dt}$ *for concentration* $\boldsymbol{x}$ *varying from 1 to 0.*

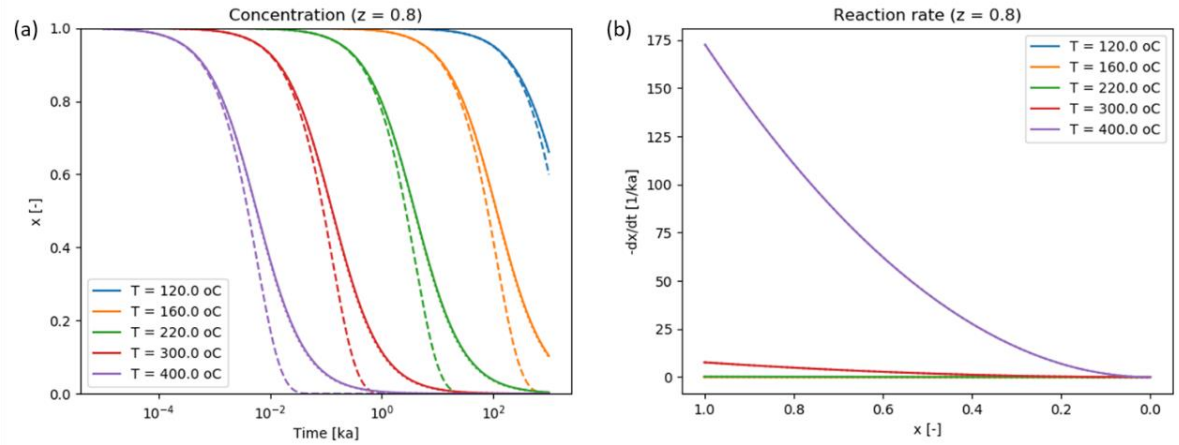

Figure 7. Analytical solution (solid line) and numerical solution (dotted line) for constant temperatures and degree of oxidation $\boldsymbol{z = 0.8}$*. (a) Concentration as function of time. (b) Reaction rate* $\boldsymbol{-dx/dt}$ *as function of concentration* $\boldsymbol{x}$*. The dashed line indicates a first order model with* $\boldsymbol{k_1 = k_2}$*.*

In the general case, the reaction rates k_1 and k_2 are given by the Arrhenius equation, with a time dependent thermal history. Then the kinetic model must be solved numerically (*Figure* ***8***). Starting from the initial condition $x = x_0 = x(t_0)$ at time $t = t_0$, a numerical solution can be obtained by the iteration,

$$E_2(n+1) = E_1 + \mu[1 - x(n)], \tag{24}$$

$$k_1(n+1) = Ae^{-\frac{E_1}{RT(n+1)}}, \tag{25}$$

$$k_2(n+1) = Ae^{-\frac{E_2(n+1)}{RT(n+1)}}, \tag{26}$$

$$\hat{k}(n+1) = \frac{1}{x_0}[k_1(n+1) - k_2(n+1)]x(n) + k_2(n+1), \tag{27}$$

$$x(n+1) = x(n)e^{-\hat{k}(n+1)dt(n+1)}, \tag{28}$$

where n is the iteration counter. The kinetic equation is stiff, with rapid changes at small times, and small changes at larger times. Therefore, it is advantageous to use a variable timestep $dt(n+1)$, increasing with iteration n. For constant temperature, the numerical solution compares well with the analytical solution (*Figure* ***9***).

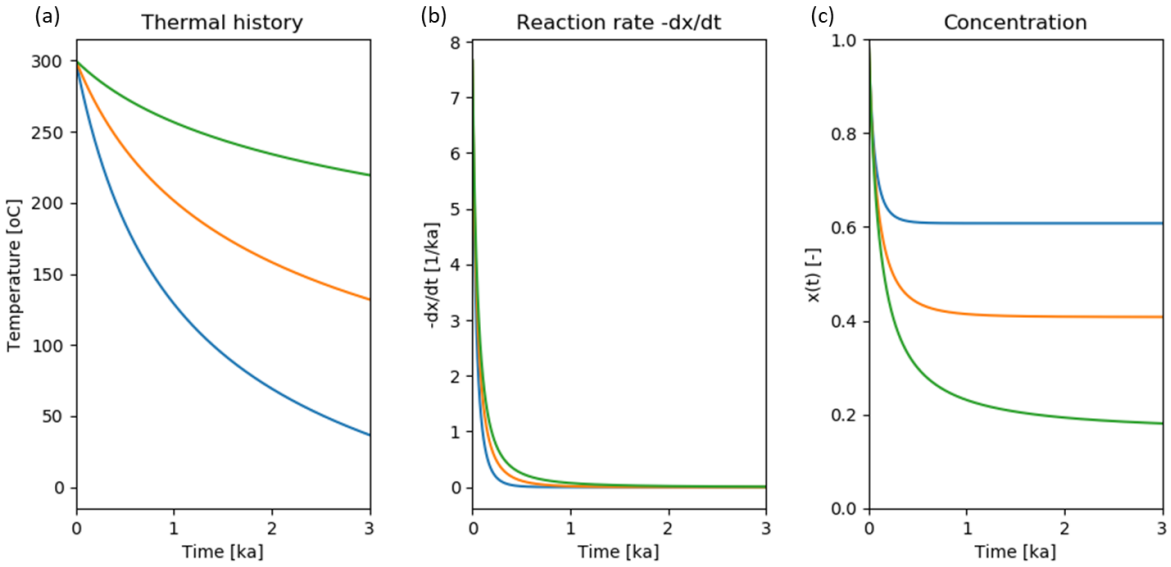

Figure 8. Numerical solutions to the mixed-order kinetic equation. (a) Thermal history, (b) Rate of change in concentration $-\boldsymbol{dx/dt}$*, and (c) concentration.*

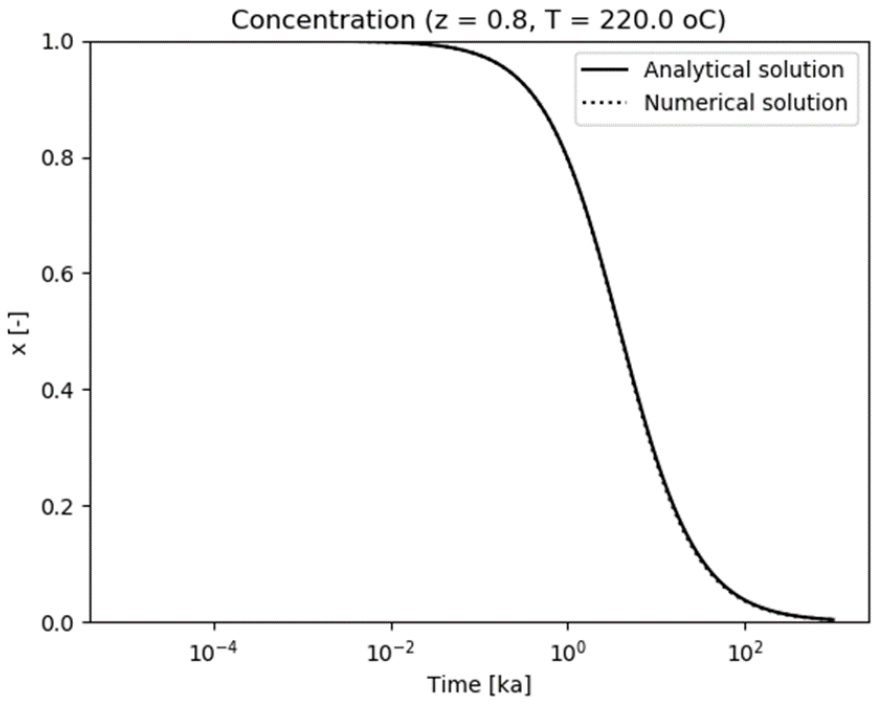

Figure 9. Comparison of analytical solution (solid line) and numerical solution (dotted line) for constant temperature $\boldsymbol{T = 220\ ^{o}C}$. *(see also dotted lines in Figure 7).*

7 Solid exsolution of titanomagnetite

When an igneous rock forms by crystalization of magma, titanomagnetite forms as a solid solution of ulvöspinel and magnetite (Butler, 1992). When the rock cools, solid exsolution takes place as follows (*Figure* ***10***): Assume that a homogeneous single-phase solid solution is formed at temperature T_0 with initial fractions u_0 and v_0 of the two species, ulvöspinel and magnetite. Upon subsequent cooling to temperature T, the solid solution enters the miscibility gap, where it becomes unstable. and decompose by spinodal decomposition, in two new phases with compositions u_1, v_1 and u_2, v_2, respectively. The phases may continue to decompose by binodal decomposition to phases with compositions $u_3, v_3$and u_4, v_4, however this relies on nucleation, associated with an activation energy, and is a much slower process (Yund and McAllister, 1969; Farjas and Roura, 2006; Wise et al., 2011). From mass conservation, u and v are not independent, and the system can be described by one of them.

For young, fast-cooling lavas, spinodal decomposition is the relevant mechanism (Smith, 1980). The spinodal decomposition is controlled by the Gibbs free energy. For the simplest model, Gibbs free energy and the spinodal are symmetric around $u = 1/2$, as in the conceptual picture in *Figure* ***10***. Laboratory studies on spinodal decomposition of titanomagnetites presented by Wise et al. (2011), shows that the spinodal does not have this symmetry (*Figure* ***11***). Gibbs free energy for a two-component solution consists of an enthalpy term and an entropy term (Miracle and Senkov, 2017). In an external magnetic field, the entropy of the magnetite will be lower than the entropy of ulvöspinel, because magnetite is magnetic, whereas ulvöspinel is not. This asymmetry can be captured if we express the Gibbs free energy G of the system as

$$G(u,v,T) = Wuv + k_B T[(1+h)u\ \mathrm{ln}u + (1-h)v\ \mathrm{ln}\ v], \quad (29)$$

where u is the fraction of ulvöspinel and v is the fraction of magnetite. By mass conservation, we then obtain the condition $u + v = 1$ and $\partial \mathrm{u} / \partial \mathrm{v} = -1$. Moreover, W is the mixing-enthalpy parameter, k_B is the Boltzmann constant, and the parameter h accounts for different magnetic entropies of magnetite and ulvöspinel.

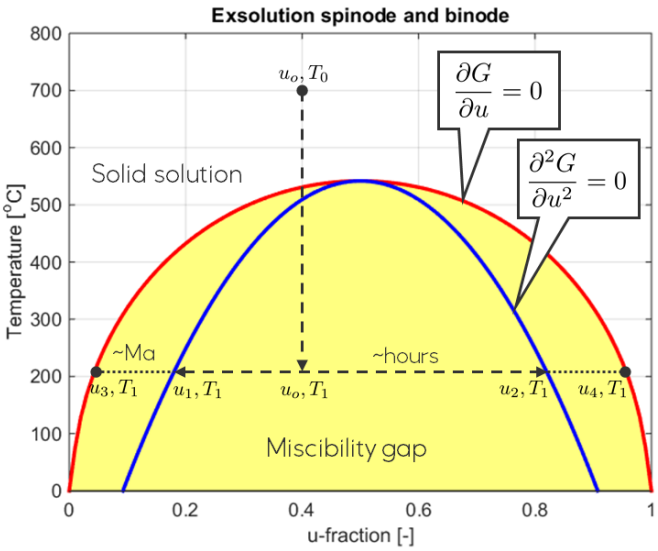

Figure 10. Exsolution binode $\frac{\partial G}{\partial u} = 0$ *(red) and spinode* $\frac{\partial^2 G}{\partial u^2} = 0$ *(blue). The yellow area marks the miscibility gap. See main text for explanation.*

The first and second derivatives of the Gibbs free energy with respect to u are obtained as

$$\frac{\partial G}{\partial u} = -\mathrm{W}(u - v) + k_B \mathrm{T}[(1 + h) ln\, u - (1 - h) ln v + 2h], \tag{30}$$

$$\frac{\partial^2 G}{\partial u^2} = -2W + k_B T \left[\frac{(1 + h)}{u} + \frac{(1 - h)}{v}\right]. \tag{31}$$

The spinodal decomposition takes place when $\frac{\partial^2 \mathrm{G}}{\partial \mathrm{u}^2} < 0$, and terminates at the spinodal equilibrium defined by $\frac{\partial^2 \mathrm{G}}{\partial \mathrm{u}^2} = 0$ (Yund and McAllister, 1969). Equation (**31** is a square equation for u, with two roots u_1 and u_2, for two different solid solutions with different magnetite and ulvöspinel fractions. Setting $h = 0$, the spinodal is symmetric around $u = 1/2$ (*Figure* ***10***). The parameters W and h can be adjusted to fit the spinodal model to the experimental measurements of Wise et al. (2011). For a given temperature, the model then predicts the equilibrium fractions of ulvöspinel and magnetite for the phases with composition u_1 and u_2, respectively (*Figure* ***11***b).

From Equation (**3** we obtain the corresponding Curie temperatures of the two phases.

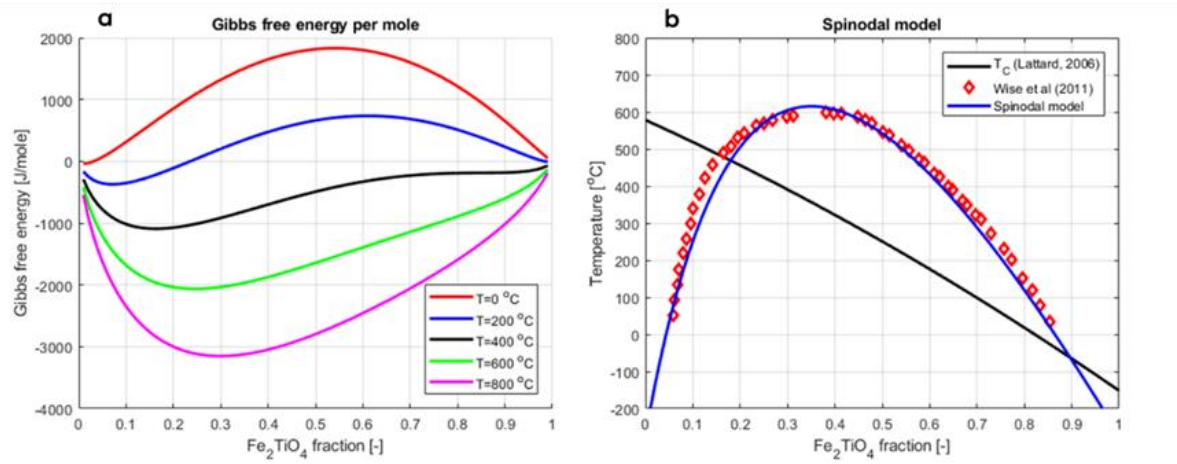

Figure 11. (a) Gibbs free energy as function of ulvöspinel fraction for various temperatures. (b) Model spinode (blue) calibrated to experimental results for titanomagnetite (red diamonds) presented by Wise et al. (2011). Also shown is the Curie temperature $\boldsymbol{T_C}$ *of titanomagnetite (black) published by Lattard et al. (2006).*

8 Oxygen fugacity and partial pressure

In addition to temperature, oxygen fugacity f_{O_2} , or partial pressure, is an important factor for oxidation processes. Quantitative studies on the effect of oxygen fugacity consider processes operating on various buffer equilibria.

Giggenbach (1987) argues that the most suitable parameter for describing the redox potential of natural fluids is

$$R_H = ln\left(\frac{f_{H_2}}{f_{H_2O}}\right). \tag{32}$$

He proposed that the redox potential of geothermal systems is controlled by the $FeO-FeO_{1.5}$ buffer equilibrium, which can be expressed as

$$2FeO + H_2O = 2FeO_{1.5} + H_2, \tag{33}$$

$$2FeO + \frac{1}{2}O_2 = 2FeO_{1.5}, \tag{34}$$

and that oxygen fugacity can be linked to temperature by the empirical relation (fugacity in MPa, T in Kelvin)

$$\ln f_{O_2} = 22.42 - \frac{58518}{T}. \tag{35}$$

D'Amore and Gianelli (1984) presented a second order polynomial in $1/T$,

$$\ln f_{O_2} = -11.07 - \frac{31564}{T} - \left(\frac{2185}{T}\right)^2. \tag{36}$$

In this model, the oxygen fugacity is low, compared to other magmatic gases (*Figure* ***12***).

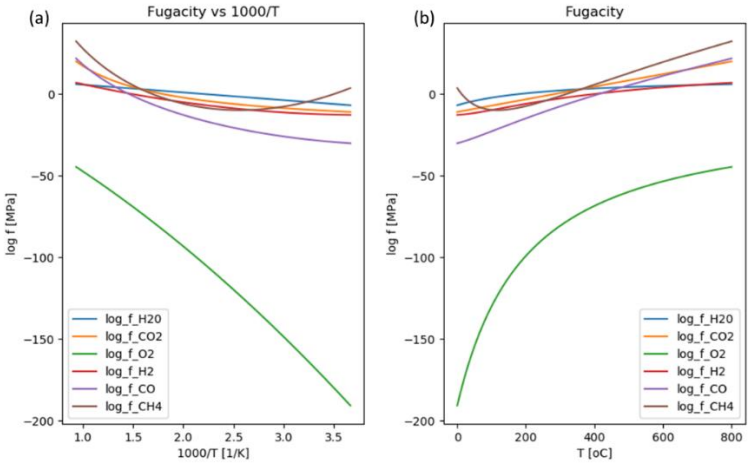

Figure 12. Fugacity of oxygen and some other magmatic gases. (a) $\ln f_{O_2}$ *vs* $1000/T$*. (b)* $\ln f_{O_2}$ *vs temperature* T *(natural logarithm).*

The Shomate equation gives enthalpy and entropy as a polynomial in $\tau = T/1000$,

$$H = a\tau + \frac{1}{2}b\tau^2 + \frac{1}{3}c\tau^3 + \frac{1}{4}d\tau^4 - \frac{e}{\tau} + f, \tag{37}$$

$$S = a\ln\tau + b\tau + \frac{1}{2}c\tau^2 + \frac{1}{3}d\tau^3 - \frac{e}{2\tau^2} + g, \tag{38}$$

where H is enthalpy (in kJ/mol) and S is entropy (in J/Kmol). The Shomate coefficients and formation enthalpy for various species of interest are given in *Table 1*.

Table 1. *Parameters for the Shomate equation. Data from the National Institute of Standards (2022).*

	O2	H2	H2O_gas	H2O_liq	CO2	CO	H2S	SO2	Fe3O4	Fe2O3
a	30.03235	18.56308	30.092	-203.606	24.997	25.568	26.884	21.43049	104.2096	93.43834
b	8.772972	12.25736	6.833	1523.29	55.187	6.096	18.678	74.35094	178.5108	108.3577
c	-3.98813	-2.85979	6.793	-3196.41	-33.691	4.055	3.434	-57.7522	10.6151	-50.8645
d	0.788313	0.268238	-2.534	2474.455	7.948	-2.671	-3.379	16.35534	1.132534	25.58683
e	-0.7416	1.97799	0.082	3.855326	-0.137	0.131	0.136	0.086731	-0.9942	-1.61133
f	-11.3247	-1.14744	-250.881	-256.548	-403.608	-118.009	-28.912	-305.769	-1163.34	-863.209
g	236.1663	156.2881	223.397	-488.716	228.243	227.367	233.375	254.8872	212.0585	161.0719
Hf	0	0	-241.826	-285.83	-393.522	-110.527	-20.502	-296.842	-1120.89	-825.503

Gibbs free energy is given by

$$G = H_f + H - TS, \tag{39}$$

where H_f is the formation enthalpy. For a buffer with chemical formula,

$$nX = mY + O_2, \tag{40}$$

the change in Gibbs free energy per mol is ("products minus reactants rule"),

$$\Delta G = mG_X - nG_Y - G_{O_2}. \tag{41}$$

The oxygen fugacity can then be obtained by

$$\ln f_{O_2} = ln\ \frac{C_X^m}{C_Y^n} + \frac{\Delta\ G}{RT}, \tag{42}$$

where C_X and C_Y represent the concentrations of species X and Y. The oxygen fugacities computed by the Shomate equation and empirical equation by D'Amore and Gianelli (1984) compare fairly well (*Figure 14*) The oxygen fugacity has a strong temperature dependence, with rapid increase for temperatures $T > 600\ ^oC$. This is particularly important for high-temperature oxidation and magmatic processes, and mainly takes place at temperatures higher than the ductile transition, and larger than the Curie temperature.

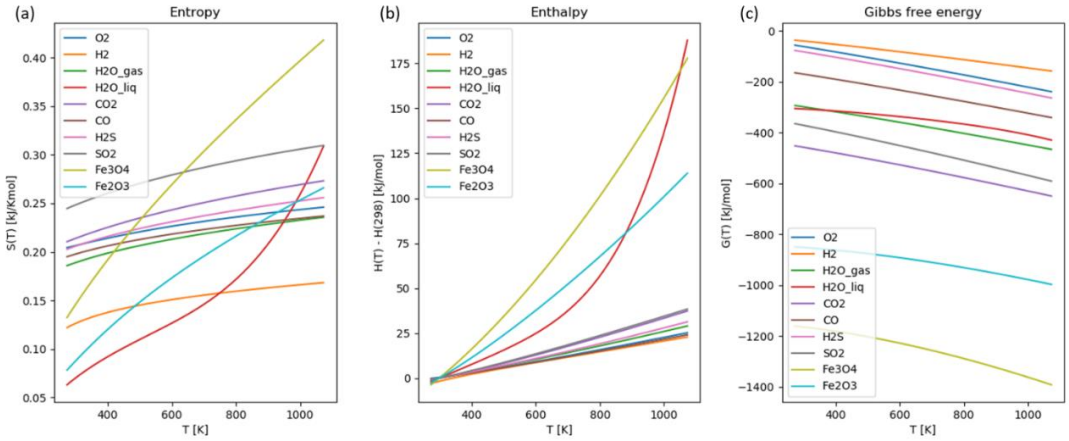

Figure 13. *Enthalpy, entropy and Gibbs free energy computed using the Shomate equation, and the coefficients given in Table 1.*

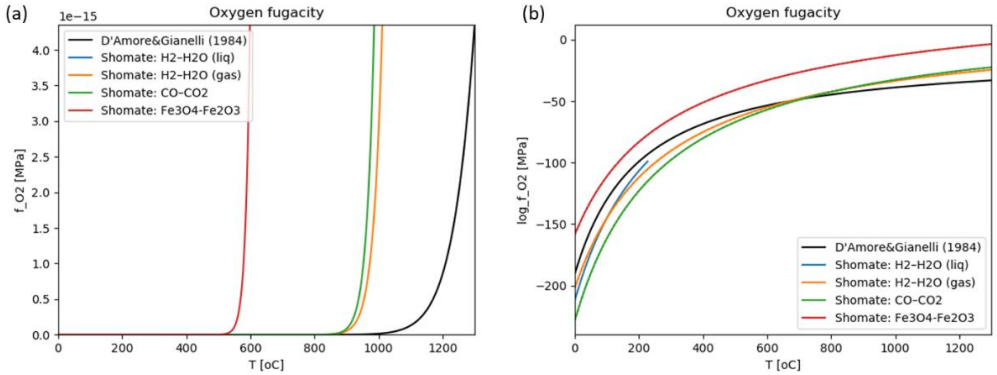

Figure 14. *(a) Oxygen fugacity and (b) log oxygen fugacity. Comparison of Shomate equation for various buffers, and the empirical relation by D'Amore and Gianelli (1984).*

When igneous rocks are cooled to temperatures below the ductile-to-brittle transition, faults and fractures become more dominant, and the system may shift from the lithostatic to the hydrostatic domain. This is associated with more efficient degassing of e.g. H_2O, CO_2, H_2S and SO_2. Hydrostatic conditions allows for influx of atmospheric (or oceanic) water, leading to higher water activity and significantly increased oxygen fugacity (Strmic Palinkas et al., 2018)

The main species of hydrothermal fluids is H_2O (water). For a system under hydrostatic conditions, the oxygen fugacity is given by

$$\ln f_{O_2} = \int \frac{V_{O_2} dp}{R\,T} \tag{43}$$

where $V_{O_2} = 32$ ml/mol is the partial molar volume of oxygen, which can be assumed to approximately constant (Ludwig and Macdonald, 2005). For low or moderate temperature gradients, such that the hydrostatic gradient

$$\frac{dp}{dz} = \rho g, \tag{44}$$

is independent of temperature, the oxygen fugacity becomes

$$ln\, f_{O_2} = \frac{V_{O_2}(P - P_0)}{R\,T} + ln(\xi P_0), \tag{45}$$

where P_0 is the pressure at the top of the hydrostatic column, and ξ is the mole fraction of oxygen. Hence, the oxygen fugacity increases with increasing pressure, and decrease with increasing temperature. If the temperature is close to the boiling temperature, hydrostatic pressure and temperature are related by the boiling curve (*Figure 15*) which can be approximated by the function

$$T(P) \simeq A[1 + B(P - P_0)]^C, \tag{46}$$

with $A = 373$, $B = 4.3$ and $C = 0.12$ (P in MPa and T in Kelvin). Then, substituting equation 46 in equation 43, the oxygen fugacity becomes

$$ln\, f_{O_2} = \frac{V_{O_2}[1 + B(P - P_0)]^{(1-C)}}{RAB(1 - C)} + ln(\xi P_0). \tag{47}$$

The boiling curve gives a lower bound on the oxygen fugacity for a column under hydrostatic pressure (*Figure **16***). For a given pressure, the oxygen fugacity decreases with increasing temperature. For a given temperature, the oxygen fugacity increases with increasing pressure.

Comparing the lithostatic and hydrostatic cases, there is a significant difference in the order of magnitude of the oxygen fugacity. This may have interesting implications for exploration for deep geothermal targets. If there is a pressure barrier separating a shallow conventional geothermal system deeper geothermal system, the two systems may have different magnetic signatures. The upper system can be expected to have a significant degree of low temperature oxidation (maghemitization), whereas the deeper system has experienced only limited high temperature oxidation of the titanomagnetite.

Thermodynamics is dealing with state variables and a system approximately in equilibrium. Kinetics is modeling the changes in concentrations. There's no straight-forward recipe for incorporating thermodynamic variables, such as

fugacity, in a kinetic model (Pekar, 2011). Data presented by can Orman and Crispin (2010) indicate that cation-diffusion rates in titanomagnetite is proportional to $f_{O_2}^{0.66} \simeq f_{O_2}^{2/3}$ (Figure 17). To incorporate the effect of oxygen fugacity in the oxidation-kinetic model, we suggest a reaction frequency factor for the Arrhenius rates given by

$$A = A_0 \phi f_{O_2}^{2/3}, \tag{48}$$

where ϕ is the porosity, and A_0 is a parameter subject to calibration.

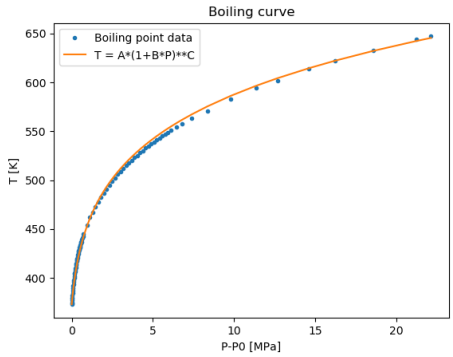

Figure 15. Boiling curve. Data from The Engineering Toolbox (blue dots), and approximated by the function $T(P) \simeq A[1 + B(P - P_0)]^C$ *(orange line).*

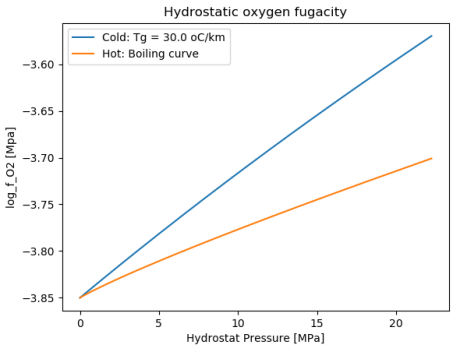

Figure 16. Natural logarithm of oxygen fugacity of a hydrostatic column. Constant thermal gradient of $\mathbf{30\ ^oC/km}$ *(blue) and on the boiling curve (orange).*

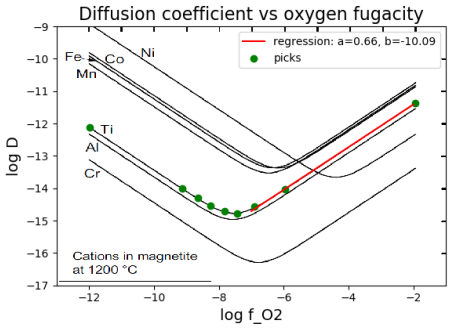

Figure 17. Cation diffusion coefficient vs oxygen fugacity. Regression line fitted to data published by van Orman and Crispin (2010). The regression line indicates that cation-diffusion rates in titanomagnetite is proportional to $f_{O_2}^{0.66}$.

9 Magnetization model for basaltic rocks

To construct a model for magnetization of basaltic rocks, we take as a starting point, magnetic minerals where the crystallization and high-temperature oxidation of magnetic minerals has already taken place. The model will take into account

- Solid exsolution of titanomagnetite
- Low-temperature oxidation of titanomagnetite
- The effect of oxygen fugacity

The signatures of the low-temperature oxidation and solid exsolution is the development of three different Curie temperatures, as discussed above, depending on the degree of oxidation, and the amount of ulvöspinel in the exsolved phases. For each Curie temperature, the magnetization is phenomenologically represented by a one-dimensonal Ising model, such that

$$M(T) = \sum_{j=1}^{3} w_j M_j\left(T; T_{cj}\right), \tag{49}$$

and

$$M_j = M_{j0} \tanh\left[\frac{T_{Cj} M_j}{T M_{j0}} + \frac{CH}{T M j_0}\right]. \tag{50}$$

The magnetization at absolute zero M_{j0}, depends on the concentration and magnetic properties of the minerals taken into account (titanomagnetite and titanomaghemite). By mass conservation and stoichiometric considerations, the weight functions w_j are obtained from the oxidation kinetics and the solid exsolution as

$$w_1 = x\frac{u_0 - u_1}{u_2 - u_1}, \tag{51}$$

$$w_2 = x\frac{u_2 - u_0}{u_2 - u_1}, \tag{52}$$

$$w_3 = x_0 - x, \tag{53}$$

$$\sum w_i = x_0, \tag{54}$$

where x is the fraction of titanomagnetite after low-temperature oxidation, u_0 is the fraction of ulvöspinel in the primary titanomagnetite (e.g. u_0 = 0.6 for for TM60), and u_1 and u_2 are the ulvöspinel fractions in the two exsolution phases, respectively. The sum of the weights sums to x_0, the initial fraction of titanomagnetite in the basalt (after high-temperature oxidation).

10 Magnetic model for the Hellisheidi and Nesjavellir geothermal areas

In 2019, Equinor performed high-resolution magnetic surveying in the Hellisheidi area. Also, a number of rock samples were collected in the lava fields. Magnetic properties were subsequently measured in co-operation with the magnetic lab at the Norwegian University of Science and Technology (NTNU) in Trondheim. Natural magnetic remanence (NRM) and magnetic susceptibility were measured at room temperature with a AGICO JR6 spinner magnetometer on one-inch plugs

drilled out of the rock samples with a titanium drillbit. Thermomagnetic measurements were performed on powder from milled basalt samples using an AGICO MFK1A Kappabridge instrument. Susceptibility was measured while heating the powder from 200 oC to +700 oC, followed by cooling back to room temperature. The high-temperature measurements were performed in inert argon atmosphere to prevent oxidation. Curie temperatures were estimated from the peaks in the thermomagnetic time series. The details of the thermomagnetic measurements are described in a separate report by ter Maat and Church (2020).

The magnetic measurements on basalt samples from Hellisheidi falls in the same range as data presented by Dietze et al (2010) and Oliva-Urcia et al. (2011). The magnetization of the young basalts from Iceland are relatively high, compared to a worldwide database of mid-oceanic ridge basalts (*Figure 18*). Most basalt samples from the Hellisheidi geothermal area reveal 2 or 3 different Curie temperatures (.

Chemical species analysis was performed on some of the samples from the Hellisheidi geothermal area. EDS scans was run on selected thin sections with focus on the magnetic mineralogy (Figure 21). In some samples, ilmenite lamella from high-temperature oxidation can be observed (Figure 21a). Plotting the theoretical mass ratios (O, Ti, Fe) for titanomagnetites with varying ulvöspinel fractions and degree of oxidation together with laboratory measurements, indicates a varying degree of oxidation (Figure 22). This is in agreement with the thermomagnetic measurements, comparing Figure 22 with Figure 20c and Figure 20f.

Table 2, *Figure* ***19***a), as was also observed at Reykjanes (Dietze et al., 2010) and in the Krafla area (Oliva-Urcia et al., 2011). Measured NRM at Hellisheidi is in the range ~5 A/m to ~50 A/m (*Figure* ***19***b). The Koenigsberger ratio is high (*Figure* ***19***d), indicating that the magnetization is mainly due to NRM. Almost all thermomagnetic curves show some degree of non-reversibility, indicating maghemitization (*Figure* ***20***). Maghemitization is also in agreement with observed Curie temperatures in the range 200-450 ºC (*Figure* ***2***b). Curie temperatures below 200 ºC and above 500 ºC can be associated with titanomagnetite.

In a few samples a peak in the thermomagnetic curves at $T \sim -150\ ^{o}C$ were observed. This can be interpreted as a Verwey transition ($T_V \simeq -150\ ^{o}C$), indicating the presence of end-member magnetite (.

Chemical species analysis was performed on some of the samples from the Hellisheidi geothermal area. EDS scans was run on selected thin sections with focus on the magnetic mineralogy (Figure 21). In some samples, ilmenite lamella from high-temperature oxidation can be observed (Figure 21a). Plotting the theoretical mass ratios (O, Ti, Fe) for titanomagnetites with varying ulvöspinel fractions and degree of oxidation together with laboratory measurements, indicates a varying degree of oxidation (Figure 22). This is in agreement with the thermomagnetic measurements, comparing Figure 22 with Figure 20c and Figure 20f.

Table 2). Also, this temperature is close to the Curie temperature of ulvöspinel.

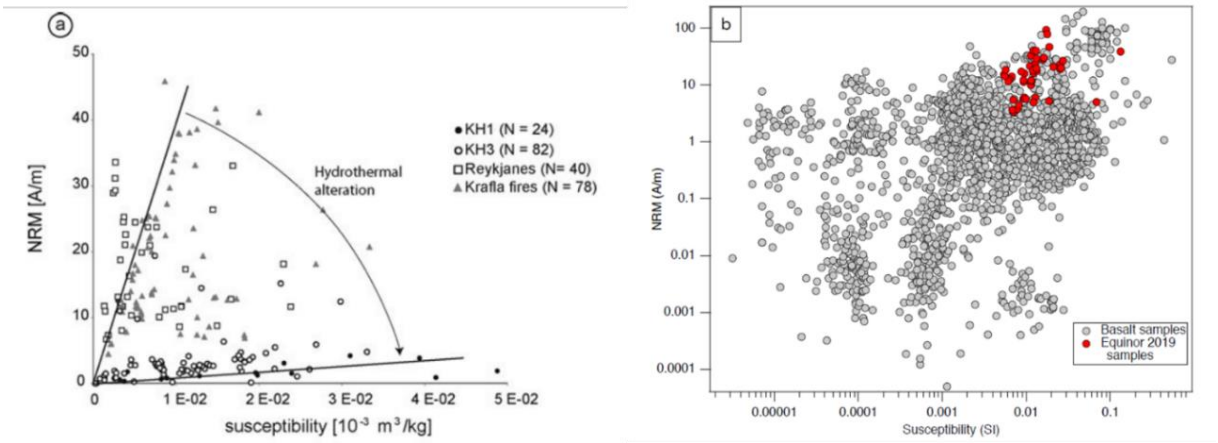

Figure 18. Magnetic properties of basaltic rocks from geothermal areas in Iceland. (a) Samples from Krafla and Reykjanes (figure from Oliva-Urcia et al., 2011). (b) Samples from Hellisheidi, collected by Equinor, lab measurements by. NTNU (ter Maat and Church, 2020), compared to a worldwide database of mid-oceanic ridge basalts from the literature.

Chemical species analysis was performed on some of the samples from the Hellisheidi geothermal area. EDS scans was run on selected thin sections with focus on the magnetic mineralogy (Figure 21). In some samples, ilmenite lamella from high-temperature oxidation can be observed (Figure 21a). Plotting the theoretical mass ratios (O, Ti, Fe) for titanomagnetites with varying ulvöspinel fractions and degree of oxidation together with laboratory measurements, indicates a varying degree of oxidation (Figure 22). This is in agreement with the thermomagnetic measurements, comparing Figure 22 with Figure 20c and Figure 20f.

Table 2. Magnetic measurements on samples from Hellisheidi. Samples collected by Equinor in August 2019 on Reykjavik Energy acreage. Lab measurements performed by NTNU (ter Maat and Church, 2020). Columns are sample ID, density, Curie tempratures (Tc1-Tc4), Verwey transition temperature (Tv), NRM, susceptibility and Königsberger ratio (Qk).

Label	dens	Tc1	Tc2	Tc3	Tc4	Tv	NRM	susc	Qk
	[kg/m3]	[oC]	[oC]	[oC]	[oC]	[oC]	[A/m]	[SI]	[-]
442	2463			469	553	-144	14.1	0.011	30.0
443	2472	60	357	462			13.7	0.009	35.3
444	2716	156	357	462			20.9	0.021	23.4
445	2505	62			548		12.8	0.006	47.0
446	2650	100			516		5.5	0.012	10.4
448	2841	111			539	-150	5.2	0.019	6.6
453	2657	60		489	545	-138	3.9	0.008	11.8
454	2663		242	498	559	-172	5.8	0.010	14.4
455	2482	87		492	541		4.7	0.027	4.1
457	2356		249	471	553		20.8	0.026	19.1
459-H1	2379	153		489	536		63.4	0.014	104.2
459-V1	2448			404			30.4	0.072	9.9
459-V2	2324		397				23.0	0.018	30.3
459-H	2365	191	343	485	564		45.9	0.014	77.3
460	2298	189		435	511		29.4	0.016	43.3
463	2224	130		435	511		11.9	0.012	24.4
464	2200	140		473	561		16.2	0.006	68.6
466	2173		391				43.7	0.016	64.5
467	2623	115		479	557		24.6	0.013	43.9

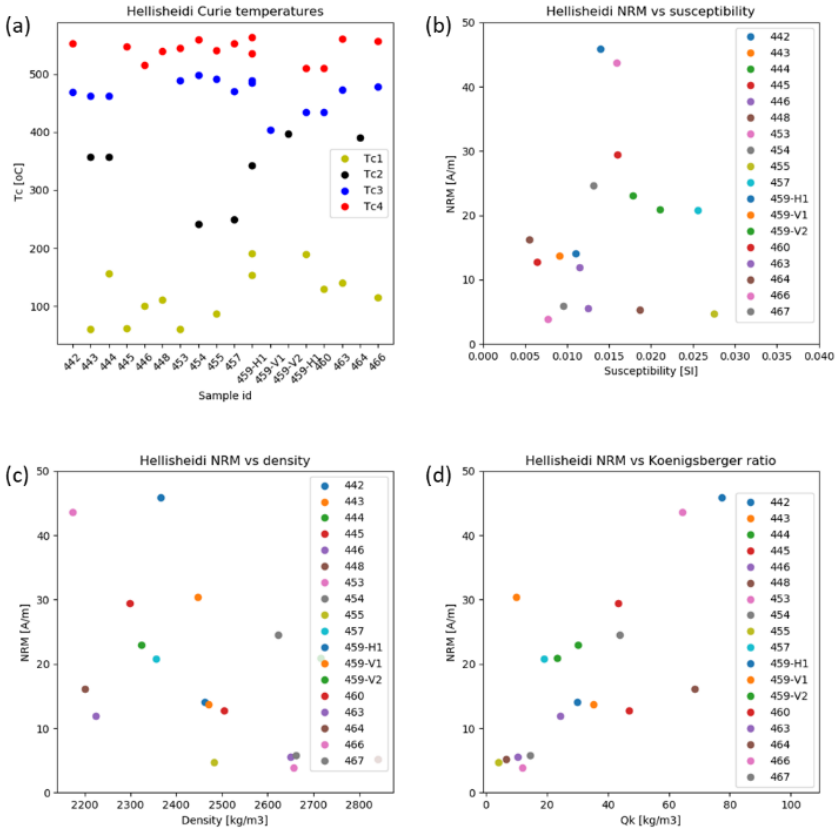

Figure 19. Magnetic measurements on samples from Hellisheidi. Samples collected by Equinor in August 2019 on Reykjavik Energy acreage. Lab measurements performed by NTNU (ter Maat and Church, 2020).

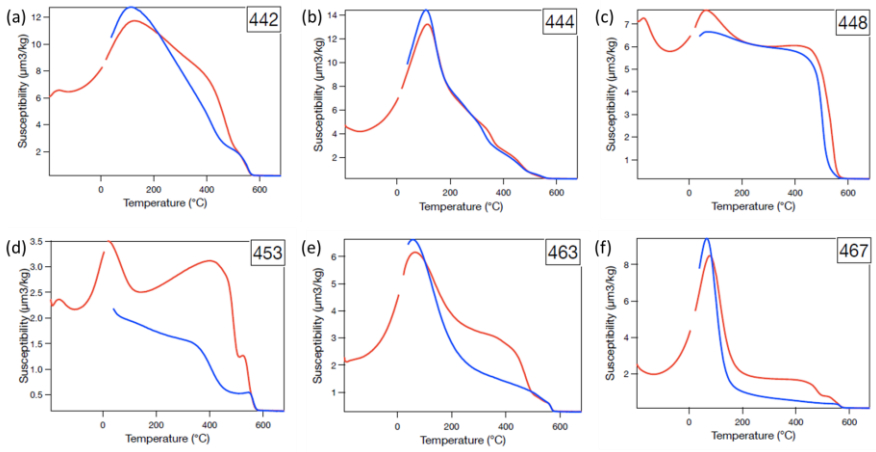

Figure 20. Representative examples of thermomagnetic curves. Susceptibility was measured while heating (red curves) powder from milled basalt samples in the temperature range -200 °C to +700 °C, followed by cooling (blue curves) back to room temperature. Laboratory measurements by NTNU (ter Maat and Church, 2020). Curie temperatures are observed as peaks in the thermomagnetic curves. End member low and high degree of maghemitization can be observed in (b) and (d), respectively. Verwey transitions are seen in (c) and (d).

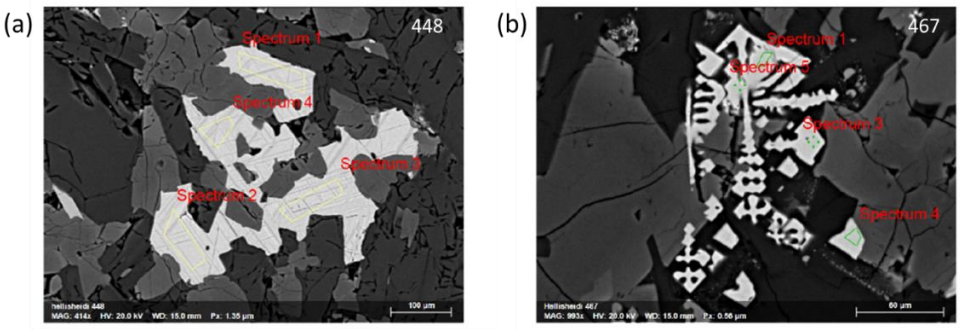

Figure 21. Images of thinsections used in EDS species analysis. The Titanomagnetites are the lighter areas. (a) Sample 448, and (b) sample 467.

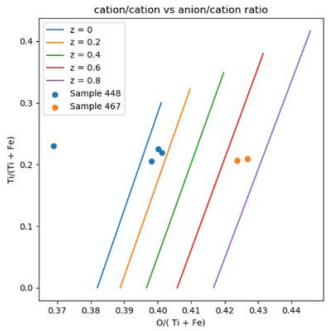

Figure 22. Mass fraction ratios Ti/(Ti+Fe) vs O/(Ti+Fe). Colored lines show theoretical mass fractions for titanomagnetite with ulvöspinel fraction varying from 0 to 1, and varying degrees of oxidation (z=0, 0.2, 0.4, 0.6, 0.8). Dots are laboratory data from EDS analysis.For the EDS scans shown, the residual species (i.e. the species that are not O, Ti or Fe) is 2-3%.

First, the magnetization model proposed above was applied to the temperature curve predicted by Hokstad and Tänavsuu-Milkeviciene (2017) for the IDDP-2 well at Reykjanes, and an exponentially decaying porosity curve (*Figure 23*). For comparison, the model was also applied for a constant temperature gradient of 45 ^{o}C/km (Figure 24). In both case, three Curie temperatures develops, varying with subsurface temperature, and the highest magnetization is obtained in the shallow colder zone. The degree of oxidation increases, and the magnetization decreases with increasing subsurface temperature. Also, the magnetization increases with a lower initial ulvöspinel-fraction in the titanomagnetite (Figure **25**).

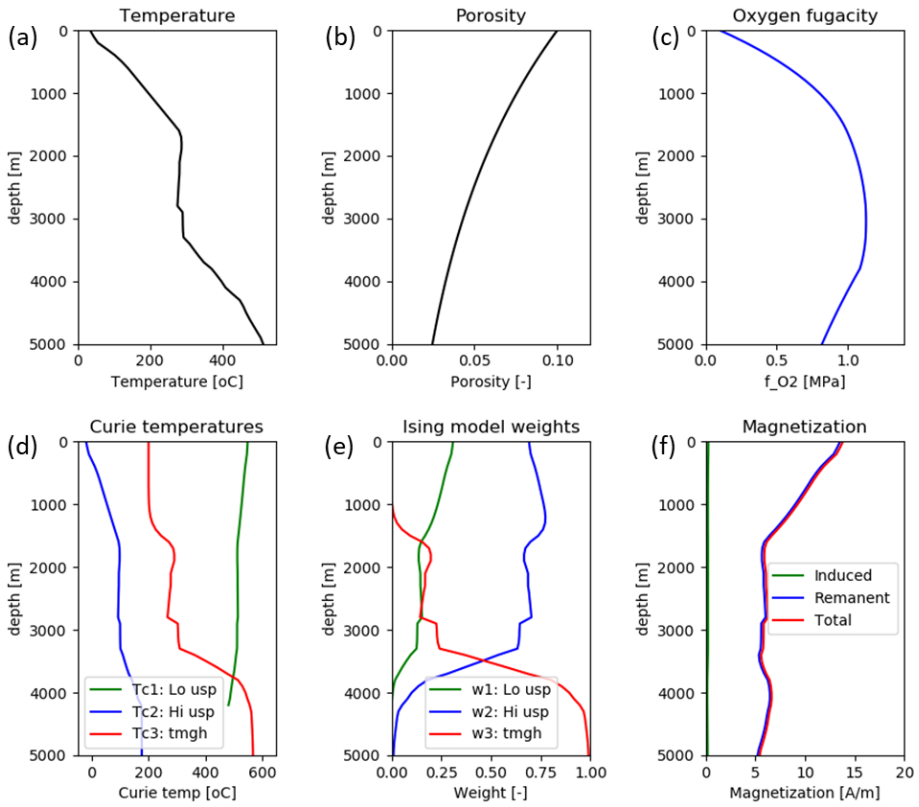

Figure 23. *Magnetic properties forward modeled using the temperature profile estimated from geophysical data at IDDP-2 well location, Reykjanes (Hokstad and Tänavsuu-Milkeviciene, 2017). (a) Temperature vs depth, (b) porosity, (c) hydrostatic oxygen fugacity, (d) Curie temperatures, (e) weights of the Ising models for each Curie temperature, and (f) Magnetization.*

Second, the magnetization model is demonstrated on a 3D cube extending from Skalafell in the south to Thingvellavatn in the north and covering the Hellisheidi and Nesjavellir geothermal areas. A 3D magnetization model was computed based on a 3D temperature cube provided by Reykjavik Energy (Figure 26 and Figure 27). Again, an exponentially decaying exponential was used (in lack of a better option). Parameters for the Ising model will normally be part of a local calibration based on available data. In the present example, the parameters were chosen as $M_0 = 40,20$ A/m for low-ulvöspinel and high-ulvöspinel titanomagnetites, $M_0 = 10$ A/m for titanomaghemite, $C = 1/(2H_0)$, and $H_0 = 42.2$ A/m. The initial ulvöspinel-fraction (after high-temperature oxidation) was chosen as $u_0 = 0.5$. The magnetic model shows reduced magnetization in the high-temperature zone, as expected. Also, ferromagnetism vanishes at temperatures higher than the Curie temperature of magnetite (575 ^{o}C)

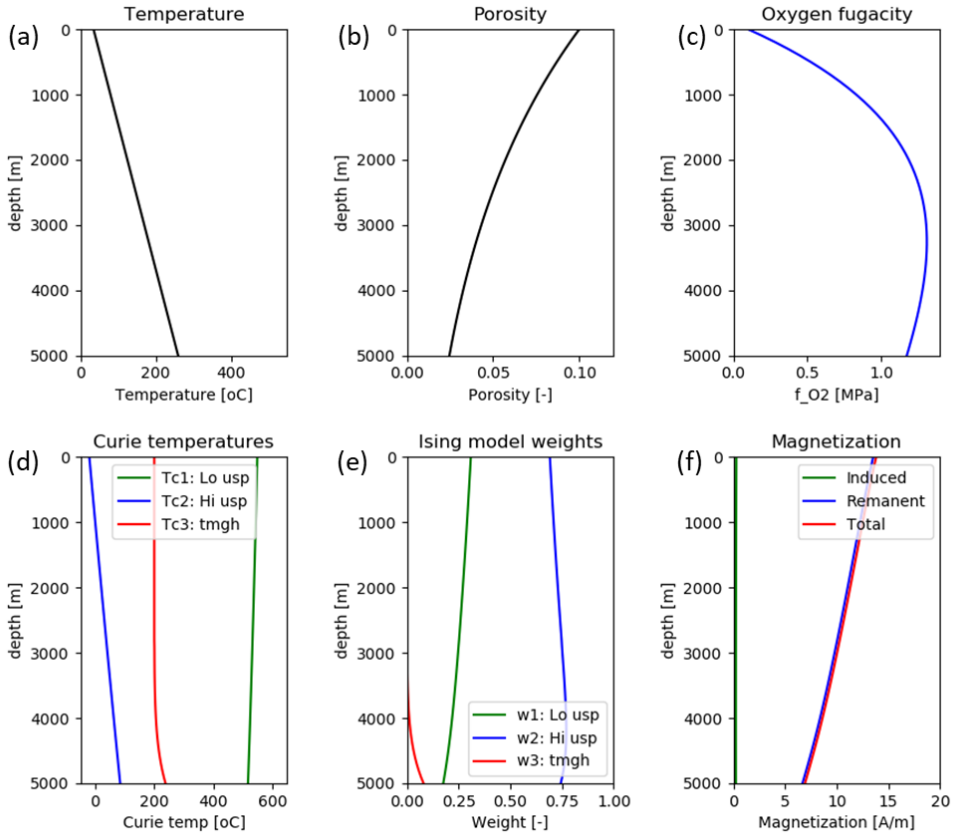

Figure 24. Magnetic properties forward modelled with a constant thermal gradient of 45 ºC/km, for comparison with Figure 23.

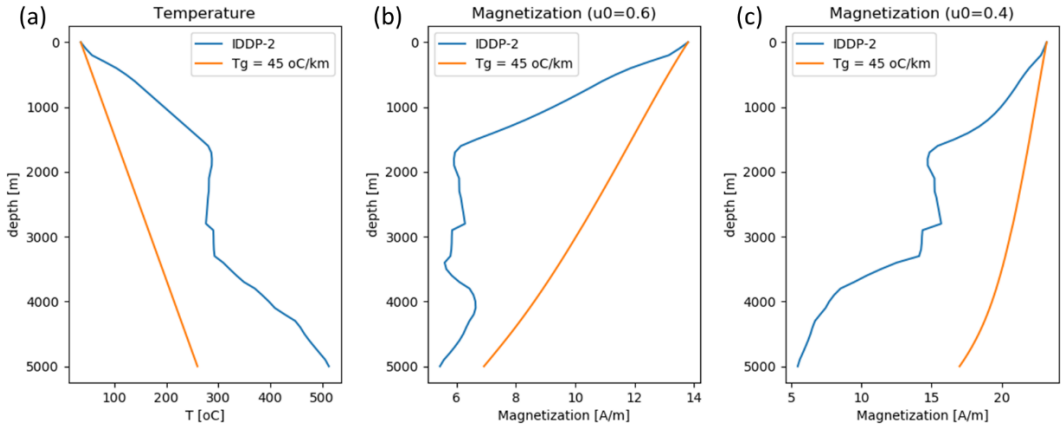

Figure 25. Comparison of magnetization for IDDP-2 temperature profile and constant thermal gradient. (a) Temperature profiles, (b) Magnetization for $\boldsymbol{u_0 = 0.6}$ (c) Magnetization for $\boldsymbol{u_0 = 0.4}$.

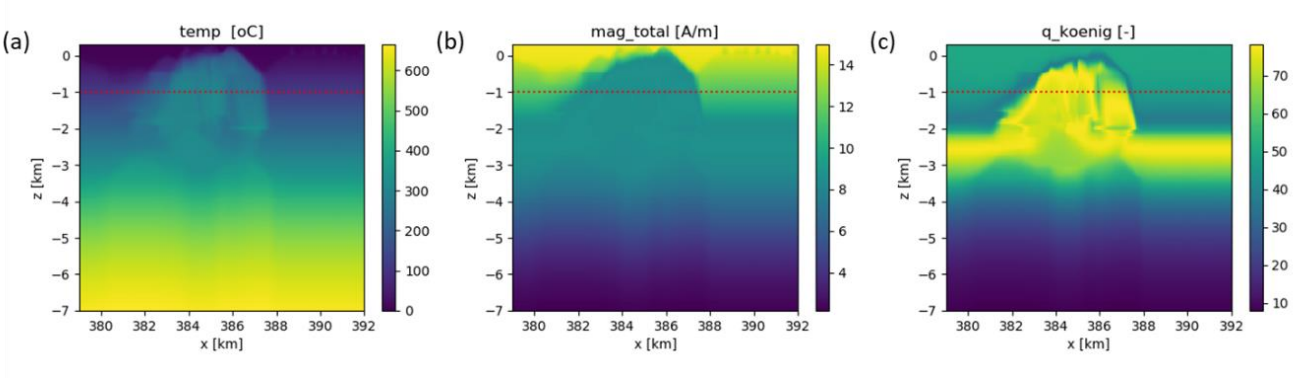

Figure 26. Vertical slice through the location of the Hellisheidi powerplant. (a) Temperature, (b) total magnetization, and (c) Königsberger ratio.

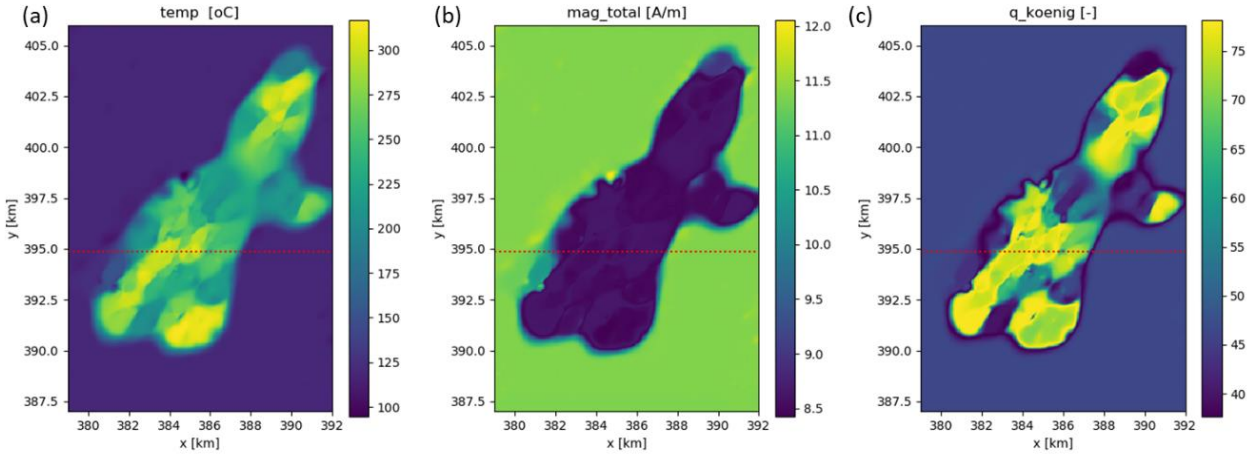

Figure 27. Horizontal slice at 1 km depth. (a) Temperature, (b) total magnetization, and (c) Königsberger ratio.

11 Conclusions

The primary carrier of magnetization in basalts is titanomagnetite, which crystalizes from magma at a temperature of 1200-1300 ºC. The titanomagnetite is oxidezed in two different stages. Fist, high temperature oxidation takes place at temperatures above 600-700 ºC. The result of the high-temperature oxidation is ilmenite lamella, and titanomagnetite with reduced titanium content. The second stage of oxidation takes place at temperatures below 300-400 ºC, and is ehanced in an acquaous environment, and rock-fluid interactions. Titanomagnetite forms as a homogenous solidsolution of ulvöspinel and magnetite. When the lava cools, the solid solution becomes unstable, and decomposes into two phases, one enriched in magnetite, the other enriched in ulvöspinel.

A mathematical model for magnetization in titanomagnetites was presented. The model takes as starting point, the titanomagnetite resulting from early high-temperature oxidation. The model describes quantitatively, the solid exsolution and the low temperature oxidation. The main chemical product of the low-temperature oxidation is titanomaghemite, a cation-deficient oxide with spinel structure. The oxidation and solid exsolution leads to three different Curie temperatures, depending on ulvöspinel fraction and the degree of oxidation. This is in agreement with thermomagnetic lab studies performed on samples from geothermal areas in Iceland (Dietze et al., 2010;

Oliva-Urcia et al, 2011; ter Maat and Church, 2020). The magnetization is modelled as a superposition of three Ising models, with relative weights depending on temperature, degree of oxidation and oxygen fugacity.

The quatitative magnetization model is demonstrated on a temperature vs depth curve from the IDDP-2 well at Reykjanes, and for a 3D temperature cube covering the Hellisheidi and Nesjavellir geothermal areas.

Oxidation and alteration of magnetic minerals is very complex process, with many possible products, including titanomagnetite, ilmenite, pseudo-brookite, rutile and clay minerals. To describe the full complexity in a quantitative model is probably not possible, and not even desired. In the present work, the goal has been to develop a model that captures first order effects, such that the model is applicable to inversion of magnetic data, multigeophysical inversion, machine learning, and geothermal exploration.

The oxidation and alteration of magnetic minerals links to subsequent chemical reactions with H2S, and the formation of metal-sulfides. Hence, the proposed model is also relevant for deep-sea mineral exploration.

12 Acknowledgments

This work was performed within the EU Geothermica project DEEPEN (WP 5), Grant Agreement No 731117.

13 References

Ade-Hall, J.M., Palmer, H.C., and Hubbard, T.P., 1971, The magnetic and opaque petrological response of basalts to regional hydrothermal alteration, Geophys. J. R. Astr. Soc., **24**, 137-174

Butler, R.F., 1992, Paleomagnetism: Magnetic Domains to Geologic Terranes. Blackwell Scientific Publications.

D'Amore F. and Gianelli G., 1984, Mineral assemblages and oxygen and sulfur fugacities in natural water-rock interaction processes. *Geochim. Cosmochim. Acta* **48**, 847-857.

Dietze, F., A. Kotny, I. Heyde, and C. Vahle, 2010, Magnetic anomalies and rock magnetism of basalts from Reykjanes (SW-Iceland): Studia Geophysica et Geodaetica, **55**, 109-130.

Fabian, K, and Shcherbakov, V.P., 2020, The magnetization of the ocean floor: Stress and fracturing of titanomagnetite particles by low-temperature oxidation, Geophys. J. Int., **221**, 2104-2112. doi: 10.1093/gji/ggaa142

Farjas, J., and P. Roura, 2006, Modification of the Kolmogorov-Johnson-Mehl-Avrami rate equation for non-isothermal experiments and its analytical solution: Acta Materialia, **54**, 5573-5579.

Gaillard, F., Scaillet, B., Pichavant, M., and Iacono-Marziano, G., 2015, The redox geodynamics linking basalts and their mantle sources through space and time. Chemical Geology, **418**, 217-233, doi: 10.1016/j.chemgeo.2015.07.030

Gapeev, A.K., and Gribov, S.K., 1990, Kinetics of single-phase oxidation of titanomagnetite, Physics of the Earth and Planetary Interiors, **63**, 58-65.

Giggenbach W.F., 1987, Redox processes governing the chemistry of fumarolic gas discharges from White Island, New Zealand. *Appl. Geochem.* **2**, 143-161.

Hokstad, K., Tašárová, Z.A., Clark, S.A., Kyrkjebø, R., Duffaut, K., Fichler, C. & Wiik, T. 2017: Radiogenic heat production in the crust from inversion of gravity and magnetic data. Norwegian J. of Geology **97**, 241–254.

Hokstad, K., and K. Tänavsuu-Milkeviciene, 2017, Temperature prediction by multigeophysical inversion: Application to the IDDP-2 well at Reykjanes, Iceland: GRC Transactions, **42**, 1141- 1152.

Hokstad, K., Alasonati Tašárová, Z., Sæther, B., and Tänavsuu-Milkeviciene, K., 2020, Inversion of Magnetic Data for Subsurface Temperature. Proceedings of the World Geothermal Congress.

Ising, E., 1925, Beitrag zur theorie des ferromagnetismus: Z.Phys, **31**, 253-258.

Johnson, H.P., and Hall, J.M., 1978, A detailed rock magnetic and opaque mineralogy study of basalts from Nazca Plat. Geophys. J. R. astr. Soc., **52**, 45-64.

Lattard, D., Sauerzapf, U., and Kasemann, M., 2005, New calibration data for the Fe-Ti oxide thermo-oxybarometers from experiments in the Fe-Ti-O system at 1 bar, 1000-1300 °C and a large range of oxygen fugacities, Contrib. Mineral Petrol, **149**, 735-754. doi: 10.1007/s00410-005-0679-2

Lattard, D., R. Engelmann, A. Kontny, and U. Sauerzapf, 2006, Curie temperatures of synthetic titanomagnetites in the Fe-Ti-O system: Effects of composition, crystal chemistry, and thermomagnetic methods: J. Geophys. Res., **111**.

Ludwig H., and Macdonald, A.G., 2005, The significance of the activity of dissolved oxygen, and other gases, enhanced by high hydrostatic pressure. Comp. Biochem. and Physiology, Part A, **140**, 387-395. doi:10.1016/j.cbpb.2005.02.001

Miracle, D., and O. Senkov, 2017, A critical review of high entropy alloys and related concepts: Acta Materialia, **122**, 448-511.

Moskowitz, B.M., and Banerjee, S.K., 1981, A Comparison of the Magnetic Properties of Synthetic Titanomaghemites and Some Oceanic Basalts. J. Geophys. Res., **86**, 11869-11882.

National Institute of Standards, 2022, NIST Chemistry WebBook, NIST Standard Reference Database Number 69. doi: https://doi.org/10.18434/T4D303

Oliva-Urcia, B., Kontny, A., Vahle, C., and Schleicher, A.M., 2011, Modification of the magnetic mineralogy in basalts due to fluid–rock interactions in a high-temperature geothermal system (Krafla, Iceland). Geophys. J. Int., 186, 155-174.

Pariso, J.E., and Johnsen, H.P., 1991, Alteration Processes at Deep Sea Drilling Project/Ocean Drilling Program Hole 504B at the Costa Rica Rift: Implications for Magnetization of Oceanic Crust, J. Geophys. Research, **B7**, 11703-11722.

Pekar, M., 2011, Thermodynamics and Reaction Rates, *in* Moreno-Pirajan, J.C. (ed), Thermodynamics - Interaction Studies - Solids, Liquids and Gases. IntechOpen. doi: 10.5772/22798

Prevot, M, Lecaille, A., and Mankinen, E.A., 1981, Magnetic effects of maghemitization of oceanic crust, J. Geophys. Res., **86**, 4009-4020.

Smith, P., 1980, Spinodal decomposition in a titanomagnetite: American Mineralogist, **65**, 1038- 1043

Steinthorsson, A., and Sveinbjørnsdottir, A.E., 1981, Opaque minerals in geothermal well no. 7, Krafla, Northern Iceland, J. of Volcanology and Geothermal Research, **10**, 245-26.

Strmic Palinkas, S., Peltekovski, Z., Tasev, G., Serafimoviski, T., Smajgl, D., Rajic, K., Spangenberg, J., Neufeld, K., and Palinkas, L., 2018, The Role of Magmatic and Hydrothermal Fluids in the Formation of the Sasa Pb-Zn-Ag Skarn Deposit, Republic of Macedonia, Geosciences **8**, 444; doi:10.3390/geosciences8120444

Ter Maat, G., and Church, N., 2020, Advanced Magnetics Solutions. Report 2, Part 1: Laboratory study on basaltic Rocks. NTNU, unpublished report contracted by Equinor.

Van Orman, J.A., and Crispin, K.I., 2010, Diffusion in Oxides. Reviews in Mineralogy & Geochemistry, **77**, 757-825.

Xu, W., D. Peacor, W. Dollase, R. Van Der Voo, and R. Beaubouff, 1997, Transformation of titanomagnetite to titanomaghemite: A slow, two-step, oxidation-ordering process in MORB: American Mineralogist, **82**, 1101-1110.

Vine, F., and D. Matthews, 1963, Magnetic anomalies over oceanic ridges: Nature, **199**, 947-949.

Wise, A., Saenko, M., Velazquez, A.M., Laughlin, D.E., Diaz-Michelena, M., and McHenry, M.E., 2011, Phase Evolution in the Fe_O_–Fe_TiO_ Pseudo-Binary System and Its Implications for Remanent Magnetization in Martian Minerals. IEE Transactions on Magnetics, **47**, 4124-4127.

Yund, R., and R. McAllister, 1969, Kinetics and mechanisms of exsolution: Chemical Geology, **6**, 5-30.'

Zhou, W., van der Voo, R., Peacor, D.R., Wang, D., Zhang, Y., 2001, Low-temperature oxidation in MORB of titanomagnetite to titanomaghemite: A gradual process with implications for marine magnetic anomaly amplitudes. J. Geophys. Res., **106**, 6409-6421.